Research Article | Vol. 27, No. 11 | 27 May 2019 | OPTICS EXPRESS 16258
Optics EXPRESS

Polarizing beam splitter cube for circularly and elliptically polarized light

SAWYER MILLER,* XINGZHOU TU, LINAN JIANG, AND STANLEY PAU

James C. Wyant College of Optical Sciences, University of Arizona, 1630 E. University Blvd., Tucson, AZ 85721, USA
*samiller@optics.arizona.edu

Abstract: A method of designing an arbitrary polarizing beam splitter (PBS) cube using multiple layers of thin-film liquid crystal polymer is demonstrated. This methodology utilizes cholesteric phase liquid crystal polymer (Ch-LCP) to transmit one handedness of elliptically polarized light and reflect the orthogonal state when unpolarized light is incident. Using additional nematic liquid crystal polymer layers, the polarization state for the transmitted and reflected light can be controlled and output to any two orthogonal states represented on the Poincaré sphere. Two cubes are designed, fabricated, tested, and compared with theory. One cube is constructed with a single layer of Ch-LCP, and another cube is constructed with a layer of Ch-LCP and an additional nematic liquid crystal polymer layer.

1. Introduction

Polarizing beam-splitter (PBS) cubes are essential components in many optical systems including: polarimeters [1], interferometers [2, 3], microscopes, display, and imaging instruments. Conventional PBS cubes, such as the MacNeille design [4], are based on numerous layers of thin-films between the two right-angle prisms of the cube [5–8]. Such devices are only operational for linear polarization states. Capasso and colleagues demonstrated arbitrary elliptical polarization beam control using metamaterials; however, these devices, as presented, require the use of high resolution micro- and nano-lithographic and patterning techniques for fabrication [9]. Other devices have been reported to utilize metamaterials and liquid crystal polymer (LCP) for use in polarization gratings for polarization control, but these devices have not been demonstrated for elliptical polarization [10, 11]. Finally, Azzam proposed a design using chiral thin-films to extend the PBS cube to circularly polarized states [12]. In this work, we consider the design and fabrication of a PBS cube where unpolarized light is input, and any two orthogonal polarization states, including circular and elliptically polarized states, are selectively transmitted or reflected out of the cube. This designed cube has elliptical states as eigenpolarizations and is analogous to the traditional MacNeille style PBS cube which has *s*- and *p*-states as eigenpolarizations, where eigenpolarization is defined as an eigenvector of the Mueller matrix [13]. The novel PBS cube is made of thin-films of LCPs sandwiched between two right-angle prisms and can separate the output to any polarization state represented on the Poincaré sphere [14]. Two different PBS cubes operating at specific wavelength and polarization states are designed, fabricated, and tested. The results are compared with theoretical calculations.

2. Theory of arbitrary PBS cube

The design of the PBS cube centers around cholesteric liquid crystal polymer (Ch-LCP), a phase of liquid crystal in which the LCP director orientation, $\hat{n}$, is continuously changing, tracing out a helical pattern described by Eq. (1) [15, 16].

#362222 https://doi.org/10.1364/OE.27.016258
Journal © 2019 Received 15 Mar 2019; revised 6 May 2019; accepted 7 May 2019; published 23 May 2019

Optics EXPRESS

$$\hat{n} = \begin{bmatrix} \cos(q_0 z) \\ \sin(q_0 z) \\ 0 \end{bmatrix}, \quad q_0 = \frac{2\pi}{p} \tag{1}$$

Here, q_0 or chirality, is defined as a function of the pitch, p, of the Ch-LCP, and z is the vertical distance measured into the Ch-LCP film at normal incidence. The pitch, along with the indices of refraction of the Ch-LCP film in the planar state (n_e, n_o), and the thickness of the film determine the reflection and transmission characteristics of the cholesteric film. If the chirality of the film is on the order of the wavelength of incident light, the Bragg condition is met, and constructive interference occurs. At normal incidence, the Ch-LCP film transmits and reflects orthogonal circular polarization states. As the angle of incidence increases, these states become elliptically polarized. To model the polarization properties of the thin-film interface in the cube, Mueller calculus [13, 17] and the Berreman 4×4 method [16, 18–22] are used. The Berreman 4×4 method breaks the cholesteric film into small slices, allowing each slice to be treated as a homogenous, nematic LCP layer. There is a slight twist in fast-axis orientation between adjacent nematic LCP layers, which allows the film's chirality to be taken into account. From here, Maxwell's equations can then be solved through each layer and also propagated to the next layer. With electric and magnetic field values known throughout the entire film, a Jones matrix and thus a Mueller matrix can be then calculated as a function of the refractive indices (n_e and n_o of the film in the planar state), pitch p of the cholesteric film, the indices of refraction surrounding the cholesteric film, and the angle of incidence of the incoming light. To achieve any output polarization state in reflection and transmission, additional layer(s) of nematic LCP acting as linear retarders can be added above and below the Ch-LCP film. These additional nematic LCP layers will rotate the elliptical eigenpolarizations of the cholesteric film to the final output polarization states. A full schematic of how the Ch-LCP thin-films are modelled is shown in Fig. 1. The Berreman 4×4 method slices the Ch-LCP film and adds a twist between adjacent layer LC directors, $\hat{n}$. A nematic LCP layer used to rotate the polarization state to the desired state is shown at the bottom of the Fig. 1.

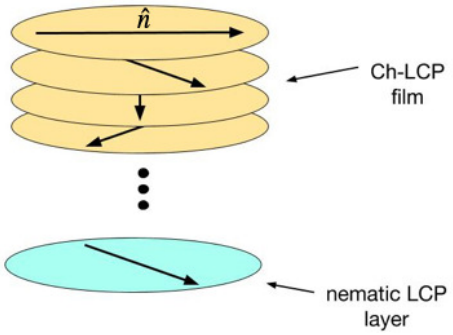

Fig. 1. The Berreman 4×4 method allows the Ch-LCP film (yellow) to be broken down into slices with varying LC director, $\hat{n}$. An additional nematic LCP layer (blue) can be added to rotate the transmitted polarization state to any state desired.

The transmitted and reflected polarization states can be calculated using the Berreman 4×4 method and then corrected with the aforementioned nematic LCP layers for the desired output polarization state and orientation. Figure 2(a) shows how a traditional MacNeille style PBS with arbitrary linear polarization input state can split the output into reflected s- and transmitted p-components. Figure 2(b) shows how a Ch-LCP PBS cube splits unpolarized light, $\vec{S}_I$, into

Optics EXPRESS

elliptical states with opposite handedness, $\vec{S}_{O,T}$ and $\vec{S}_{O,R}$. The transmitted and reflected output states can then be rotated to any orthogonal polarization states with additional retarder layers. Arbitrarily polarized light can be input into the Ch-LCP PBS cube as well. Varying irradiance values for $\vec{S}_{O,T}$ and $\vec{S}_{O,R}$ will be output depending on the input polarization state just as varying irradiance values for s- and p-components will be output with a MacNeille PBS cube for an arbitrary input polarization state. A family of possible variations of this design is represented by the red (transmitted state, $\vec{S}_{O,T}$) and green (reflected state, $\vec{S}_{O,R}$) points. In Fig. 2(b), the fast-axis orientation and magnitude of retardance are changed to generate the possible polarization states. It is stressed that the possible variations in design are not limited to those represented in Fig. 2(b).

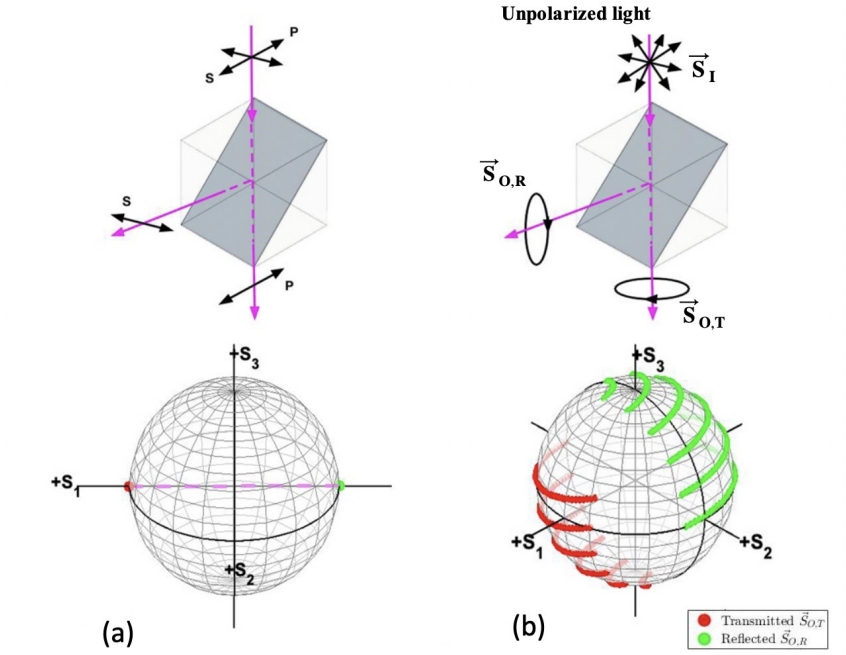

Fig. 2. (a) A traditional MacNeille style PBS cube splits an arbitrary linear polarization state into orthogonal s- and p-components, shown as diametrically opposite points on the Poincaré sphere. (b) An arbitrary PBS cube splits unpolarized light, $\vec{S}_I$, into orthogonal transmitted and reflected elliptical states, $\vec{S}_{O,T}$ and $\vec{S}_{O,R}$, respectively. The Ch-LCP PBS cube splits arbitrary input polarization states as well, with the transmitted and reflected irradiance depending on the input polarization. Additional retarder layers can be added to allow any orthogonal polarization states to be transmitted or reflected. A set of possible polarization states is shown on the Poincaré sphere at bottom right. Each set of orthogonal points represents a PBS cube with different nematic LCP layer thicknesses and fast-axis orientations.

3. Two PBS designs

In this study, PBS cubes of single and dual-layer of LCP operating at a specific narrow wavelength band were designed and fabricated.

3.1. Single-layer PBS cube

The first cube was fabricated with a single layer of Ch-LCP between two prisms. Simulations using the Berreman 4×4 method were performed for the first cube, where only a Ch-LCP film

was present. Due to the positioning of film within the cube, the input light's angle of incidence relative to the film is 45°. As the angle of incidence to the film increases, the transmitted and reflected polarization states stay close to orthogonality. The Euclidean norm, $\|s\|$ was used to quantify this. In this instance, the Euclidean norm between the true orthogonal polarization state of the transmitted light and the actual polarization state of the reflected light was calculated. This is described by Eq. (2), where $\vec{S}_{O,T\perp}$ is the polarization state orthogonal to the transmitted polarization state, $\vec{S}_{O,T}$, and $\vec{S}_{O,R}$ is the reflected polarization state. For transmitted and reflected states that are perfectly orthogonal and of equal irradiance, $\|s\|$ is equal to zero in Eq. (2).

$$\|s\| = \left[\sum_{i=1}^{3}\left(S_{O,T\perp_i} - S_{O,R_i}\right)^2\right]^{1/2} \tag{2}$$

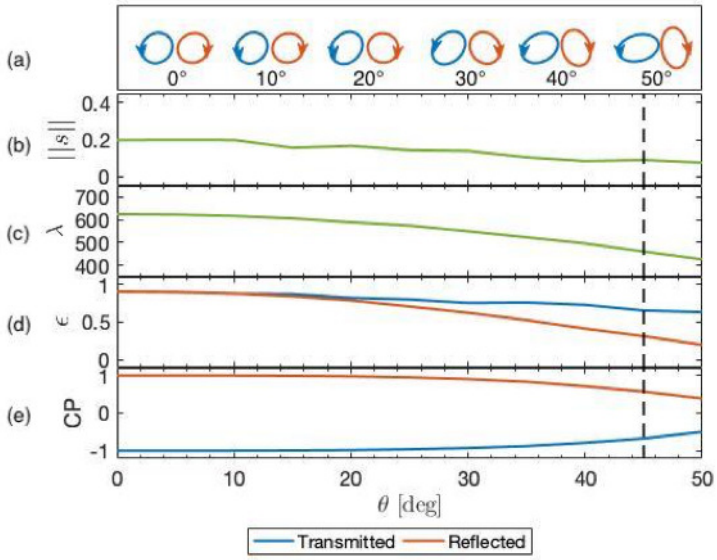

Fig. 3. Theoretical performance of the Ch-LCP film as a function of angle of incidence. The vertical dashed line marks angle of incidence of 45°, where the Ch-LCP film operates as a PBS cube. (a) Polarization ellipses are plotted for selected angles of incidence. (b) The Euclidean norm measuring the orthogonality of the polarization state between the transmitted light and the reflected light. (c) The operating wavelength shifts towards shorter wavelengths as the angle of incidence is increased. (d) The ellipticities of the transmitted and reflected beams decrease as the angle of incidence increases. (e) The circular polarizance trends toward more elliptical polarization properties as the angle of incidence increases.

Figure 3 shows the variation in the simulated polarization properties of the Ch-LCP film. Figure 3(a) plots polarization ellipses for selected angles of incidence. As the angle of incidence increases, the polarization states can be seen to become more elliptical. At 0° angle of incidence, the polarization ellipses are nearly perfect orthogonal circular states. In Fig. 3(b), the Euclidean norm between the polarization state orthogonal to the transmitted light and reflected polarization state stays close to the same value as the angle of incidence increases. At 0° angle of incidence, the Euclidean norm should be zero, as orthogonal circular states are both reflected and transmitted. At 0° angle of incidence, the calculated Euclidean norm is approximately equal to 0.2. In general, the Euclidean norm for Stokes vectors has a maximum value of two, representing a reflected state which is the exact same polarization state as the transmitted state. In our calculation, the Euclidean norm decreases from 10% to 5% of the maximum Euclidean norm value from 0°

Optics EXPRESS

to 50°. The Berreman 4×4 simulation shows these states to be almost perfectly orthogonal; thus, the non-zero Euclidean norm value. These results are in agreement with simulations performed by Yeh and Gu [18] and are a consequence of the non-orthogonality of the normal modes propagating through the Ch-LCP film in the Bragg regime. Figure 3(c) describes the shift in the peak operating wavelength, defined as the wavelength where the circular polarizance in reflection and transmission are the highest. Circular polarizance (*CP*) measures the property of an optical component, where unpolarized light is converted into circularly polarized light and is defined by $CP = m_{3,0} / m_{0,0}$ where m is a component of the Mueller matrix, and the subscript notation is consistent with Chipman [13]. Simulations show the peak operating wavelengths as defined are almost identical in transmission and reflection. Increasing the angle of incidence causes a trend toward shorter wavelengths. This is consistent with known blue-shift phenomena of thin-films. Figure 3(d) plots the ellipticities of the transmitted state (blue) and reflected state (orange). As the angle of incidence increases, the polarization states become less circular and more elliptical. The deviation from one at zero angle of incidence is also in agreement with published results in the Bragg regime [18]. Finally, in Fig. 3(e), the circular polarizance is plotted. As the angle of incidence increases, the exiting polarization state is less circular and more elliptical. The Ch-LCP in the PBS cube operates at 45° of angle of incident as marked by the dashed line. As the angle of incidence increases beyond 50°, the metric for determining the peak operating wavelength is not well-defined because the circular polarizance in transmission and reflection begin to have multiple maxima.

3.2. Dual-layer PBS cube

The second PBS cube was fabricated with additional nematic LCP layers. These additional layers were added to rotate the transmitted light to any desired polarization state and to aid the Ch-LCP in alignment. For this PBS cube, it is desired for a transmitted elliptically polarized state to be rotated to circularly polarized state. To make an achromatic PBS cube, more than one layer of nematic LCP are needed on both sides of the Ch-LCP film to rotate the transmitted and reflected states (discussed later in Section 6). For the second PBS cube, an output state of right circularly polarized light in transmission was desired. A Mueller matrix for the nematic LCP layer used for aiding the alignment of the Ch-LCP was determined by treating the layer as a linear retarder. The Mueller matrix for the linear retarder can be defined as a function of retardance, δ, and fast axis orientation, Φ, in Eq. (3).

$$LR(\delta,\Phi) = \begin{bmatrix} 1 & 0 & 0 & 0 \\ 0 & \cos^2 2\Phi + \cos\delta \sin^2 2\Phi & (1-\cos\delta)\cos 2\Phi \sin 2\Phi & -\sin\delta \sin 2\Phi \\ 0 & (1-\cos\delta)\cos 2\Phi \sin 2\Phi & \cos\delta \cos^2 2\Phi + \sin^2 2\Phi & \cos 2\Phi \sin\delta \\ 0 & \sin\delta \sin 2\Phi & -\cos 2\Phi \sin\delta & \cos\delta \end{bmatrix} \quad (3)$$

A Berreman 4×4 simulation was performed on the Ch-LCP layer using parameters of best fit found empirically with data from test wafers. The Berreman 4×4 simulation data was then used to calculate a Mueller matrix for the Ch-LCP film in transmission. Next, a Mueller calculation was performed and considers the transmission polarization output through the alignment nematic LCP layer and the Ch-LCP film. The polarization state in transmission is then rotated by a final nematic LCP layer, to the desired right circularly polarized state. Multiplying the incident unpolarized Stokes vector, $\vec{S}_I$, by the Mueller matrix describing the alignment nematic LCP layer, $LR_A(\delta,\Phi)$, the Mueller matrix Ch-LCP film in transmission, EP_{Ch-LCP_T}, and the Mueller matrix for the nematic LCP layer, $LR_R(\delta,\Phi)$, the transmitted output Stokes vector, $\vec{S}_{O,T}$, can be calculated, as shown in Eq. (4).

Optics EXPRESS

$$LR_R(\delta,\Phi)\cdot EP_{Ch-LCP_T}\cdot LR_A(\delta,\Phi)\cdot\vec{S}_I=\vec{S}_{O,T},\ \text{where}\ \vec{S}_I=\begin{bmatrix}1\\0\\0\\0\end{bmatrix} \tag{4}$$

The desired output state in transmission is right-hand circularly polarized and has a Stokes vector: $\vec{S}_{O,T} = [1\ 0\ 0\ 1]^T$. Simulations show a retardance of $\delta = 130°$ and a major axis orientation of $\Phi = 85°$ relative to the plane of tilt at 450 nm for $LR_R(\delta,\Phi)$ give a nearly perfect right-hand circular transmitted state given the specifications of $LR_A(\delta,\Phi)$ and EP_{Ch-LCP_T}.

This procedure can be extended for light reflected by the Ch-LCP film as well. The Ch-LCP film in reflection can be described by a Mueller matrix, EP_{Ch-LCP_R}. Using Eq. (4), the retardance and orientation of the nematic LCP layer, $LR_R(\delta,\Phi)$, can be calculated. $LR_R(\delta,\Phi)$ rotates the reflected light to the desired polarization state, $\vec{S}_{O,R}$. In this case, $LR_R(\delta,\Phi)$ and $LR_A(\delta,\Phi)$ describe the same nematic LCP layer only differing in describing the direction of transmission through the nematic LCP film. By using a nematic LCP film as an alignment aid, the design and fabrication process is simplified; however, this layer must be accounted for as part of Eq. (4) in the simulation.

Our PBS is currently designed for unpolarized input light; however polarized input can be accepted. The Ch-LCP layer can transmit and reflect elliptical states regardless of the input. The amount of light that is reflected or transmitted is determined by the input polarization state. Accordingly, $\vec{S}_I$ can be modified in Eq. (4) to determine the transmitted and reflected polarization states.

4. Fabrication

4.1. Methods

Photoalignment techniques developed for flat wafer substrates were successfully applied to coat surfaces of right-angle prisms using two customized polytetrafluoroethylene (PTFE) holders, a coating holder and an exposure holder. The finished, coated prisms were subsequently bonded together by optical epoxy to form the PBS cube. The photoalignment process utilizes a photoalignment material [23–25]. After exposure to linearly polarized ultraviolet (LPUV) light, the photoalignment material is patterned and serves as a template with direction perpendicular to the UV light polarization. The liquid crystal polymer is then spin-coated onto the substrate and aligned. In the dual-layer PBS cube, a nematic LCP layer is applied on top of the photoalignment layer and aid in aligning the Ch-LCP as well as rotating the polarization state of the reflected light.

4.2. Materials

The right-angle prism, made of K9 glass, has dimensions of 25.4 mm in length, width, and height. The photoalignment material used is an azo-dye, SD1 [26, 27]. SD1 is added to *N,N*-dimethylformamide in a 0.38% weight concentration ratio. The Ch-LCP is RMS09-027, designed to have a broad reflectance spectrum. There are two nematic LCPs used. The first is RMM141C, which is added to toluene in a 40% weight concentration ratio. The second is RMM1707, which is added to toluene in a 44% weight concentration ratio. All LCP materials were available from EMD Performance Materials.

Optics EXPRESS

4.3. Fabrication process

All the film coating and processing were performed on the hypotenuse face of a prism. Directions of SD1 alignment are shown for each prism in Figs. 4(a)-4(c). Fabrication processes of the single-layer cube with the Ch-LCP film are as follows:

1. The prism surface was cleaned with a rinse of acetone and isopropyl alcohol and dried with nitrogen gas. The prism was then exposed to oxygen plasma for two minutes.
2. The prism was mounted on the coating holder, as shown in Fig. 4(d), with the face perfectly leveled. The SD1 was spin coated onto the surface at 3000 RPM, 3000 RPM/s for 30 seconds.
3. The prism, in the coating holder, was baked in an oven at 150°C for five minutes.
4. The prism was removed from the coating mount and inserted into the exposure mount, which sits above a beaker of water, so the SD1 film on the prism face was kept away from water since SD1 is water soluble. The other faces of the prism were immersed in water during the LPUV exposure. This arrangement prevents the LPUV from total internal reflection at the prism's non-processing faces and scrambling the photoalignment pattern on the SD1 film.
5. The SD1 was patterned under a UV source with irradiance of 30.5 mW/cm^2 at 365 nm for five minutes. The polarizer used is a UV linear dichroic polarizer manufactured by Boulder Vision Optik. The SD1 was patterned so the fast-axis of the nematic layer is set parallel to the hypotenuse of the prism, as seen in Fig. 4(a).
6. The prism was reinserted into the coating mount, and Ch-LCP was spin coated onto the surface at 2000 RPM, 1000 RPM/s for 1 minute.
7. The prism, in the coating mount, was baked in an oven at 95°C for four minutes.
8. The Ch-LCP film was cured under the same UV source for five minutes in a nitrogen atmosphere.
9. Norland Optical Adhesive 89 was then applied on the Ch-LCP film, and a second bare prism was glued onto the processed prism to complete the PBS. The entire device was cured under a UV lamp for 10 minutes in a nitrogen atmosphere. The finished single-layer cube is shown in Fig. 4(e).

The dual-layer cube fabrication requires coatings to be performed on the faces of both prisms. Details for the dual-layer cube fabrication are as follows:

1. Prism surfaces were prepared with rinse of acetone and isopropyl alcohol and dried using nitrogen gas. Both prisms were then exposed to oxygen plasma for two minutes.
2. SD1 was then spin coated on the faces of both prisms at 3000 RPM, 3000 RPM/s for 30 seconds. Both were then baked in an oven at 150°C for five minutes.
3. For Prism #1, the SD1 was aligned using polarized UV light so the fast-axis of the nematic layer will be parallel to the hypotenuse of the prism, as shown in Fig. 4(b). For Prism #2, the SD1 was aligned so the fast-axis of the nematic layer will be at 85° to the hypotenuse of the prism, as shown in Fig. 4(c).

Optics EXPRESS

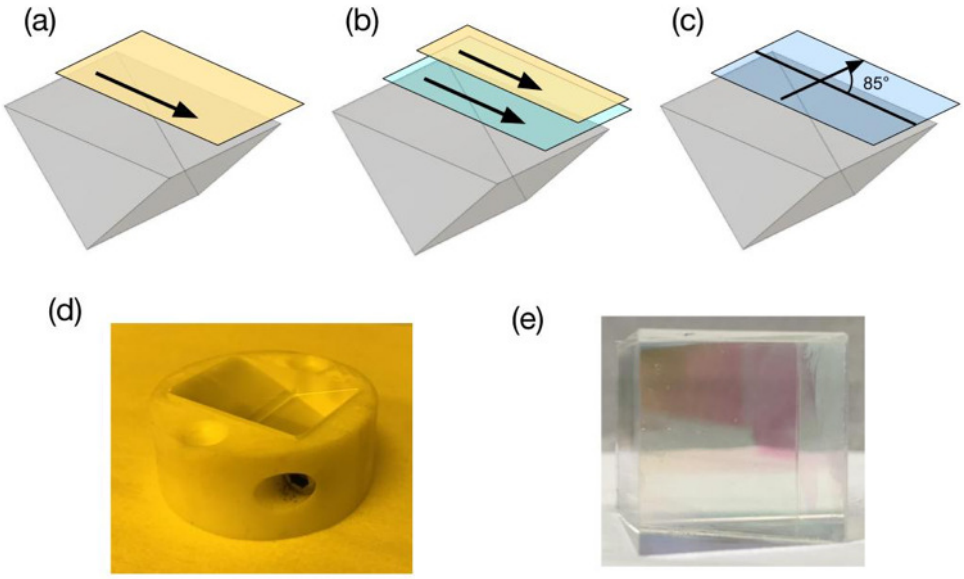

Fig. 4. (a) The alignment direction for the Ch-LCP layer on the single-layer PBS. (b) The alignment directions for the nematic LCP layer (blue) and Ch-LCP layer (yellow) are shown for the dual-layer PBS. The nematic LCP layer improves alignment of the Ch-LCP layer and rotates the polarization state of the reflected light. (c) The alignment direction for the nematic LCP layer used for rotating the polarization state to right-hand circular in transmission is shown for the dual-layer PBS. (d) Prism mount for spin coating made of PTFE is shown. (e) Finished single-layer PBS cube is shown.

4. For Prism #1, RMM141C was spin coated on the face at 4000 RPM, 2000 RPM/s for one minute. The prism then was set aside for five minutes at room temperature. This nematic LCP layer is used as an aid in aligning the Ch-LCP layer. This layer adds retardance to the beam splitter and must be accounted for in the simulation when describing the polarization in both transmission and reflection.
5. The RMM141C was then cured for five minutes under UV in a nitrogen atmosphere.
6. The Ch-LCP was spin coated on top of the cured RMM141C at 2000 RPM, 1000 RPM/s for one minute. The film was then baked in an oven at 95°C for four minutes, and then cured under UV in a nitrogen atmosphere for five minutes.
7. For Prism #2, RMM1707 was spin coated on the face at 2020 RPM, 1000 RPM/s for one minute. It then was set at room temperature for five minutes.
8. The RMM1707 film was cured under UV in a nitrogen atmosphere for five minutes.
9. Prisms #1 and #2 were then glued together using Norland Optical Adhesive 89. The entire device was then cured under UV in a nitrogen atmosphere for 10 minutes.

5. Theory and experiment of two PBS cubes

Both PBS cubes were characterized using an Axometrics Mueller matrix polarimeter and a Newport 1830-C power meter to determine polarization properties as well as irradiance values in

Optics EXPRESS

transmission and reflection. Figures 5(a) and 5(c) show the thin-film schematics for the single and dual-layer PBS cubes, respectively. The input light directions are shown in the figures as well. Figures 5(b) and 5(d) show the circular diattenuation, $CD = m_{0,3} / m_{0,0}$, of the PBS cubes in transmission (top) and reflection (bottom). The measured results from the PBS cubes are compared with the Berreman 4×4 simulation.

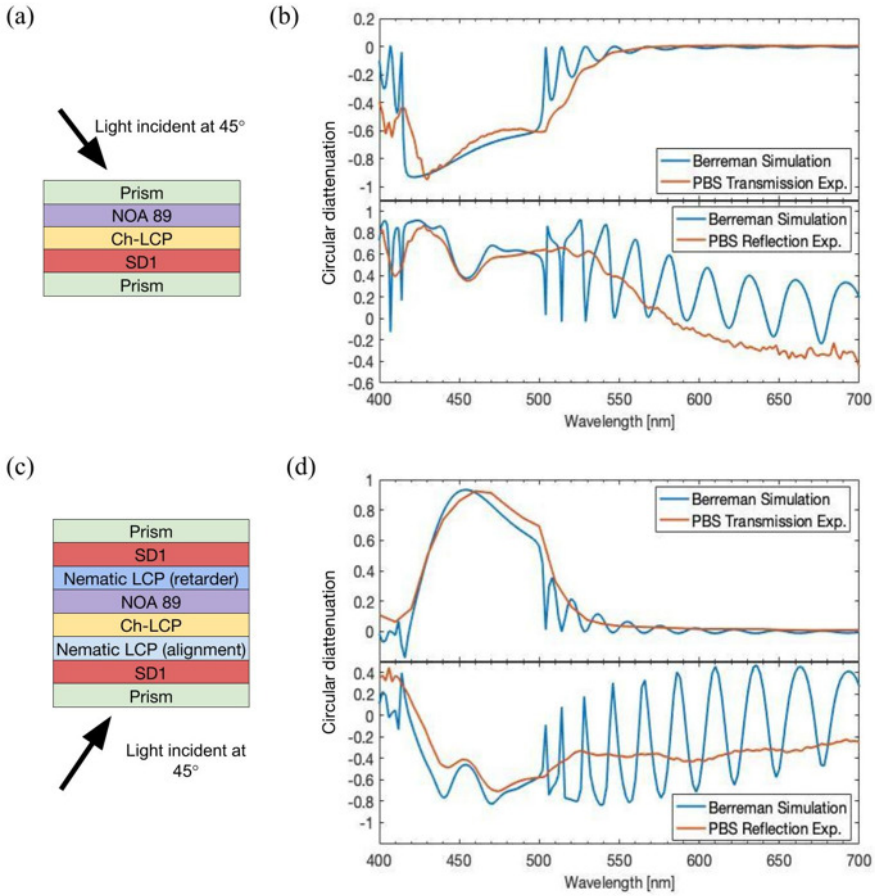

Fig. 5. (a) Single-layer PBS cube thin-film schematic. (b) Measured circular diattenuation for transmission (top) and reflection (bottom) are compared with Berreman 4×4 simulations for the single-layer PBS cube. (c) Dual-layer PBS cube thin-film schematic. (d) Measured circular diattenuation for transmission (top) and reflection (bottom) are compared with Berreman 4×4 simulations for the dual-layer PBS cube.

The single-layer PBS cube in transmission had a measured peak *CD* of -0.91 and 0.87 in reflection at 430 nm. The dual-layer PBS cube had a measured peak *CD* of 0.925 in transmission at 450 nm and -0.71 in reflection at 474 nm. These values can be seen in Figs. 5(b) and 5(d). Circular polarizance (*CP*) was measured and compared with Berreman 4×4 simulations for both cubes as well. The single-layer PBS cube had a peak *CP* in transmission of 0.89 and a peak *CP* in reflection of 0.85 both at 430 nm. Berreman 4×4 simulations produce circular polarizance values that agree well with the measured data with differences within 3% for both transmission and reflection at 430 nm. The dual-layer PBS cube had a peak *CP* in transmission of 0.956 at 450 nm and a peak *CP* in reflection of -0.77 at 474 nm. Compared to the measured results, Berreman

Optics EXPRESS

4×4 simulations produce *CP* results that are within 4% and 9% differences in transmission and reflection, respectively. Operating bandwidth for these cubes is defined over the range, where the difference in peak *CP* is within ± 5%. The single-layer PBS cube has an operating bandwidth of 427 ± 5 nm in transmission and 428 ± 2 nm in reflection. The dual-layer PBS cube has an operating band of 450 ± 10 nm in transmission and 474 ± 4 nm in reflection.

Parameters of best fit for the Berreman 4×4 simulations are given in Table 1 below.

Table 1. Parameters of best fit for Berreman 4×4 simulations

Parameter	Single-layer Cube	Dual-layer cube
n_e	1.725	1.725
n_o	1.525	1.525
Pitch	380 nm	380 nm
Ch-LCP Film thickness	~6000 nm	~6000 nm
Retarder fast axis	n/a	85°
Linear retardance	n/a	130°

Differences between theory and experiment can be attributed to three approximations in the simulations. First, the refractive indices are assumed to be independent of wavelength, i.e. no dispersion. Simulations with dispersion have been shown to have the same locations of maxima and minima as obtained from the experimental measurements [28]. Secondly, there is no absorption in the Berreman 4×4 calculations. The Norland optical adhesive is known to be absorptive in the wavelength from 400 nm to 430 nm [29]. Thirdly, the Berreman 4×4 simulation assumes a purely monochromatic light is incident. In the measurement, a tunable light source with finite bandwidth of ± 2 nm was used, and the sidelobes, with many local maxima and minima, were averaged out. Rapid oscillations at wavelengths longer than 500 nm in the reflection simulations were not observed in the measurements either, as the signal in reflection dropped off quickly past the working band of the Ch-LCP. Another observation is the sign of the circular diattenuation for the two PBS cubes. The retarder layer was designed to rotate the output polarization state from a left-handed elliptical beam to a right-hand circular state, resulting in the different sign in circular diattenuation.

Figure 6 shows the Mueller matrix for each cube in transmission and reflection as a function of wavelength. As both cubes are designed to work with unpolarized input light, the first column of the Mueller matrix or polarizer vector is of upmost importance. We consider first the single-layer PBS cube. In transmission (solid blue), the elliptical output can be seen with the values in elements $m_{2,0}$ and $m_{3,0}$ At 420 nm, where circular polarizance is maximum as shown in element $m_{3,0}$, the single-layer PBS cube also has a measurable amount of linear polarizance at 45° as shown in element $m_{2,0}$. This creates elliptically polarized light in transmission when unpolarized light is incident. Similar behavior is observed in reflectance from the single-layer PBS cube (solid orange). In the polarizer vector, elements $m_{1,0}$, $m_{2,0}$, and $m_{3,0}$ all record values of equal magnitude but with the opposite signs of the transmission data at 420 nm. This is indicative of orthogonal elliptical polarization states being transmitted and reflected.

We next consider the dual-layer PBS cube. In transmission (dashed yellow), peak circular polarizance is observed close to 450 nm. The linear polarizance depicted in elements $m_{1,0}$ and $m_{2,0}$ goes to zero near 450 nm, resulting in a perfectly circularly polarized output beam. The degree of circular polarization for this state was measured to be 0.992. Finally, we consider the

Optics EXPRESS

reflectance of the dual-layer PBS cube (dashed purple). The peak circular polarizance is observed close to 450 nm, in agreement with the transmission data. However, without the additional nematic LCP layer to rotate the final polarization state to circular in reflection, elements $m_{2,0}$ and $m_{3,0}$ both show nonzero values at 450 nm. Elliptically polarized output is recorded in reflection, as anticipated. Both cubes performed as expected and in agreement with the Berreman 4×4 simulation.

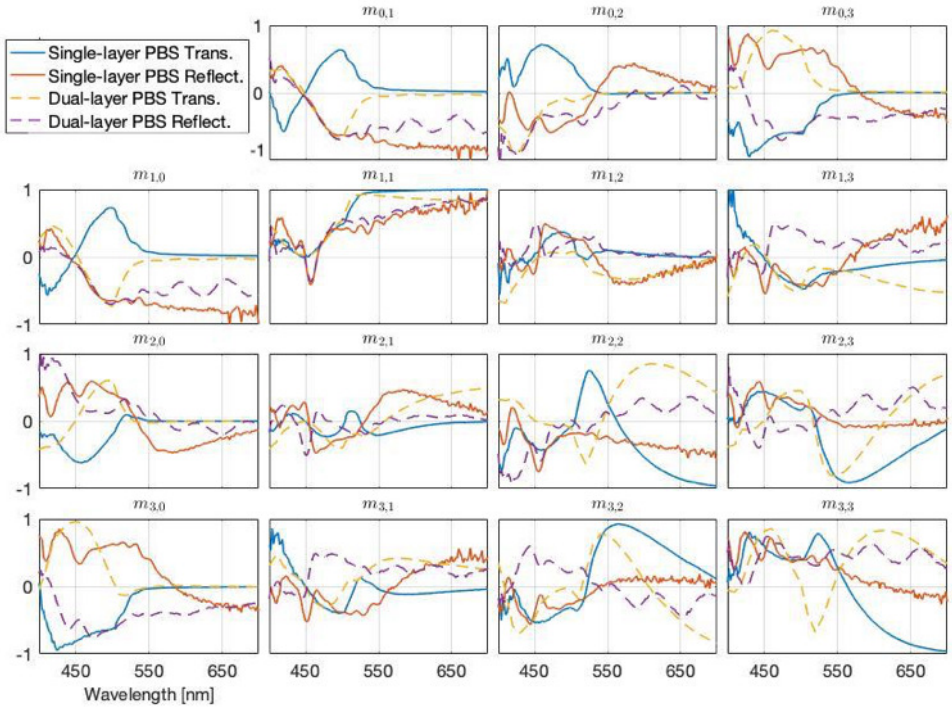

Fig. 6. Wavelength dependent Mueller matrix in transmission and reflection showing the values for each element. Element $m_{0,0}$ is omitted as a normalized Mueller matrix is depicted for each cube. The results for single-layer PBS cube are plotted with solid lines, while those for the dual-layer PBS cube are plotted with dashed lines.

For unpolarized incident light, the Euclidean norm of the transmitted and reflected light is measured to be 0.174 for the single-layer cube at 420 nm. Theory predicts a value of 0.0894. This difference can be attributed to scattering, which is measured to be 3 to 5% [15, 30] and incomplete alignment of the Ch-LCP. When the measured Stokes vectors are decomposed into fully polarized and fully unpolarized components, the Euclidean norm between fully polarized Stokes vectors is reduced to be 0.0783, which is closer to the theoretical value.

The amount of irradiance split between the transmitted and reflected beam paths were measured as well. The single-layer cube produced results that show a transmitted power of 30% and a reflected power of 38% of the incident beam at the operating wavelength of 420 nm. The prisms do not have antireflection coating, and the Fresnel transmission coefficient for two interfaces at 420 nm is 0.91. In addition to scattering from the Ch-LCP film, the Norland optical adhesive is lossy in the wavelength range of 400-430 nm. For comparison, the dual-layer PBS cube has a transmission of 32% and a reflection of 41% at the peak operating wavelength of 450 nm.

Optics EXPRESS

6. Conclusion

In this paper, PBS cubes that split unpolarized light into light of arbitrary polarization states were designed and tested. Although traditional MacNeille type PBS cubes are widely used and available, they are limited to linearly polarized light output. The extension to nonlinear output polarization states, such as elliptically and circularly polarized light, can open up new applications in display, 2D and 3D imaging, interferometry, and quantum optics. Two different PBS cubes for different polarizations were demonstrated. The first cube utilized a single-layer of Ch-LCP and split unpolarized light into two orthogonal elliptically polarized states. The second cube utilized a combination of a Ch-LCP layer and a nematic layer of LCP to split unpolarized light into circularly and elliptically polarized states. The degree of circular polarization for the transmitted beam was found to be 0.992 for the rotated state. While we have utilized only two layers in our design, additional layers can be applied to broaden the operating wavelength of the PBS and convert the reflected light to be fully orthogonal to the transmitted light. Formulation of Ch-LCP that has a chirped pitch can be applied to extend the operating wavelength of the PBS. Alternatively, wire grid polarizers, designed to have high transmission and reflection of linearly polarized states, can be combined with achromatic retarders [31–33] to create broadband PBS. Finally, PBS loss can be further reduced by antireflection coatings, application of low loss epoxy, and better alignment of liquid crystal polymer.

Funding

National Science Foundation (NSF) (1607358).

Acknowledgments

We thank the DIC Corporation for providing us photoalignment material and Barry Seff at EMD Performance Materials for supplying us RMS09-027.

References

1. V. Gamiz, "Performance of a four channel polarimeter with low light level detection," Proc. SPIE **3121**, 35–46 (1997).
2. D. Malacara, *Optical Shop Testing* (John Wiley & Sons, 2007).
3. G. Sommargren, "Phase shifting interferometer," U.S. Pat. 5,933,236 (August 3, 1999).
4. S. MacNeille, "Beam splitter," U.S. Pat. 2,403,731 (July 6, 1946).
5. M. Banning, "Practical methods of making and using multilayer filters," J. Opt. Soc. Am. **37**, 792–797 (1947).
6. L. Li and J. A. Dobrowolski, "High-performance thin-film polarizing beam splitter operating at angles greater than the critical angle," Appl. Opt. **39**, 2754–2771 (2000).
7. I. Hodgkinson, Q. H. Wu, M. Arnold, L. D. Silva, G. Beydaghyan, K. Kaminska, and K. Robbie, "Biaxial thin-film coated-plate polarizing beam splitters," Appl. Opt. **45**, 1563–1568 (2006).
8. R. M. A. Azzam, "Polarizing beam splitters for infrared and millimeter waves using single-layer-coated dielectric slab or unbacked films," Appl. Opt. **25**, 4225–4227 (1986).
9. J. P. Balthasar Mueller, N. A. Rubin, R. C. Devlin, B. Groever, and F. Capasso, "Metasurface polarization optics: Independent phase control of arbitrary orthogonal states of polarization," Phys. Rev. Lett. **118**, 113901 (2017).
10. E. Hasman, Z. Bomzon, A. Niv, G. Biener, and V. Kleiner, "Polarization beam-splitters and optical switches based on space-variant computer-generated subwavelength quasi-periodic structures," Opt. Commun. **209**, 45–54 (2002).
11. C. Oh and M. J. Escuti, "Achromatic diffraction from polarization gratings with high efficiency," Opt. Lett. **33**, 2287–2289 (2008).
12. R. M. A. Azzam, "Chiral thin solid films: Method of deposition and applications," Appl. Phys. Lett. **61**, 3118–3120 (1992).
13. R. Chipman, W. Lam, and G. Young, *Polarized Light and Optical Systems* (CRC, 2019).
14. S. Pau, "Imaging method and apparatus using circularly polarized light," U.S. Pat. Appl. 62/583,301 (2017).
15. S. Chandrasekhar and J. S. Prasad, "Theory of rotatory dispersion of cholesteric liquid crystals," Mol. Cryst. Liq. Cryst. **14**, 115–128 (1971).
16. D. Yang and S. Wu, *Fundamentals of Liquid Crystal Devices* (John Wiley & Sons, 2010).
17. R. Chipman, "Polarimetry," in *OSA Handbook of Optics,* (McGraw-Hill, 2010).
18. P. Yeh and C. Gu, *Optics of Liquid Crystal Displays*, 2nd ed. (John Wiley & Sons, 2010).
19. D. W. Berreman, "Optics in stratified and anisotropic media: 4×4-matrix formulation," J. Opt. Soc. Am. **62**, 502–510 (1972).

Optics EXPRESS

20. D. W. Berreman and T. J. Scheffer, "Reflection and transmission by single-domain cholesteric liquid crystal films: Theory and verification," Mol. Cryst. Liq. Cryst. **11**, 395–405 (1970).
21. H. Wöhler, G. Haas, M. Fritsch, and D. A. Mlynski, "Faster 4×4 matrix method for uniaxial inhomogeneous media," J. Opt. Soc. Am. A **5**, 1554–1557 (1988).
22. S. Lowrey, L. D. Silva, I. Hodgkinson, and J. Leader, "Observation and modeling of polarized light from scarab beetles," J. Opt. Soc. Am. A **24**, 2418–2425 (2007).
23. W. Hsu, J. Ma, G. Myhre, K. Balakrishnan, and S. Pau, "Patterned cholesteric liquid crystal polymer film," J. Opt. Soc. Am. A **30**, 252–258 (2013).
24. W. Hsu, K. Balakrishnan, M. Ibn-Elhaj, and S. Pau, "Infrared liquid crystal polymer micropolarizer," Appl. Opt. **53**, 5252–5258 (2014).
25. G. Hegde and L. Komitov, "Periodic anchoring condition for alignment of a short pitch cholesteric liquid crystal in uniform lying helix texture," Appl. Phys. Lett. **96**, 113503 (2010).
26. H. Akiyama, T. Kawara, H. Takada, H. Takatsu, V. Chigrinov, E. Prudnikova, V. Kozenkov, and H. Kwok, "Synthesis and properties of azo dye aligning layers for liquid crystal cells," Liq. Cryst. **29**, 1321–1327 (2002).
27. V. Chigrinov, H. S. Kwok, H. Takada, and H. Takatsu, "Photo-aligning by azo-dyes: Physics and applications," Liq. Cryst. Today **14**, 1–15 (2005).
28. R. Dreher, G. Meier, and A. Saupe, "Selective reflection by cholesteric liquid crystals," Mol. Cryst. Liq. Cryst. **13**, 17–26 (1971).
29. Norland Products Incorporated, *Norland Optical Adhesive 89H* (2018). Datasheet.
30. S. Y. Lu and R. A. Chipman, "Interpretation of mueller matrices based on polar decomposition," J. Opt. Soc. Am. A **13**, 1106–1113 (1996).
31. S. Pancharatnam, "Achromatic combinations of birefringent plates: Part 1. an achromatic circular polarizer," Proc. Ind. Acam. Sci. A **41**, 130–136 (1955).
32. C. M. McIntyre and S. E. Harris, "Achromatic wave plates for the visible spectrum," J. Opt. Soc. Am. **58**, 1575–1580 (1968).
33. X. Tu, L. Jiang, M. Ibn-Elhaj, and S. Pau, "Design, fabrication and testing of achromatic elliptical polarizer," Opt. Express **25**, 10355–10367 (2017).